A General Computational Framework for Modeling Cellular Structure and Function

James Schaff, Charles C. Fink, Boris Slepchenko, John H. Carson, and Leslie M. Loew
Center for Biomedical Imaging Technology, Departments of Physiology and Biochemistry, University of Connecticut Health Center, Farmington, Connecticut 06030 USA

ABSTRACT The "Virtual Cell" provides a general system for testing cell biological mechanisms and creates a framework for encapsulating the burgeoning knowledge base comprising the distribution and dynamics of intracellular biochemical processes. It approaches the problem by associating biochemical and electrophysiological data describing individual reactions with experimental microscopic image data describing their subcellular localizations. Individual processes are collected within a physical and computational infrastructure that accommodates any molecular mechanism expressible as rate equations or membrane fluxes. An illustration of the method is provided by a dynamic simulation of IP_3-mediated Ca^{2+} release from endoplasmic reticulum in a neuronal cell. The results can be directly compared to experimental observations and provide insight into the role of experimentally inaccessible components of the overall mechanism.

INTRODUCTION

Cellular structure and function are determined by an array of interdependent biochemical reactions and processes, spatially distributed in a nonhomogeneous fashion within the cell. There is a formidable amount of data concerning the biochemistry of cellular molecules on the one hand, and microscopic image data on the structure and behavior of cells on the other. Experimental methods such as patch clamp and site-directed mutagenesis have joined traditional biochemical and molecular biological approaches to generate an ever-expanding catalog of biomolecular reaction mechanisms and kinetics. Electron microscopy, x-ray crystallography, and NMR spectroscopy are providing an atomic-level understanding of the structure of biological macromolecules and biomolecular assemblies. Tools such as fluorescent probes and confocal microscopy have made possible the determination of three-dimensional intracellular spatial distributions of molecular species as well as subcellular structures in living cells. It should be possible to use basic physical-chemical principles to organize and understand all of these data. This problem is close to being solved at the molecular level, where it is now possible to calculate the structures and dynamics of large proteins and nucleic acids as well as their interactions with solvents, ligands, and substrates. At the level of the cell, however, there is no general approach to modeling the spatially organized and interdependent chemical processes that determine cell function. This would be desirable, not only for the purpose of testing hypotheses, but also as a means of collecting and organizing this massive quantity of experimental data.

Received for publication 26 February 1997 and in final form 29 May 1997.
Address reprint requests to Dr. Leslie M. Loew, Department of Physiology, University of Connecticut Health Center, MC3505, 263 Farmington Ave., Farmington, CT 06030-1269. Tel.: 860-679-3568; Fax: 860-679-1269; E-mail: les@volt.uchc.edu.

0006-3495/97/09/1135/12 $2.00

Most approaches to modeling cellular processes describe their system as a single set of ordinary and partial differential equations. This limits the complexity of the model with respect to interacting features of the physiological system and forces a homogeneous representation of the cellular geometry. We have developed a system, the "Virtual Cell," for building complex cell models based on a hierarchical assembly of molecules, reaction mechanisms, and their associated intracellular structures. Once the cell model is created, it serves as the input to a numerical simulation of intracellular dynamics that is calculated by using the finite-volume formalism (Patankar, 1980). This permits a spatially heterogeneous collection of volume elements in which each element is identified with the physiology of a single class of cellular features. The geometrical organization of the elements can correspond to the organization of their associated structural features in an experimental micrograph. Therefore, complex behavior may be simulated with a collection of simple models. Each simple model maps directly onto a biological feature and encapsulates only the physiology associated with that feature. A model will specify how the concentrations of molecules can change within an element and how an element might exchange molecular species with its neighbors. Thus an assembly of different elements can interact with complex behavior, even though their individual behaviors may be simple. Indeed, this organization closely approximates the actual dynamics within the cell. Comparison of simulation results and observed behavior is facilitated because the microscopy data and the simulation model are mapped onto the same geometry.

UNDERLYING PHYSICAL CONCEPTS

A key feature of the Virtual Cell is that the physical laws controlling intracellular molecular dynamics are integral to the infrastructure and do not have to be reformulated for every physiological process to be studied. Thus a physiological model can be constructed from biochemical and

biophysical knowledge of a system with the assurance that the underlying infrastructure will properly apply the appropriate physical laws. This simplifies the modeling process and makes it more accessible to the experimentalist.

The problem consists of a set of continuous partial differential equations relating the state variables of the system and the input stimuli. The formulation accounts for diffusion in the presence of concentration and/or electric gradients, chemical reactions, and membrane transactions due to pumps and channels. The set of state variables includes the concentrations of each molecular species, C_i, and the electric potential, V, defined over a subset of three-dimensional space for times greater than zero. State variables are defined such that knowledge of their values at time $t = 0$ is sufficient to determine the behavior of the whole system for any known stimulus. In general, the rules governing the state variables are a function of position (heterogeneous) and of the state variables (nonlinear).

The physical infrastructure is divided into components describing

1. molecular flux, $\vec{\mathbf{J}}_i$, of diffusible molecules dependent on concentration and electrical gradients;
2. electric flux density, $\vec{\mathbf{D}}$, dependent on the distribution of charged molecules according to the laws of electrostatics;
3. current density, $\vec{\mathbf{I}}$, defined by a cable theory formalism (Jack et al., 1975b);
4. source terms arising from reactions according to differential rate equations (Frost and Pearson, 1961); and
5. membrane transactions in which bulk concentrations of molecular species and/or electrical potential regulate membrane surface enzyme kinetics or transmembrane flux.

Components 1–4 are defined throughout the physical space, whereas membrane transactions are confined to the interfaces between distinct compartments (e.g., the plasma membrane separates extracellular and cytosolic compartments). It is important to appreciate that all of the components are interdependent. Components 1, 4, and 5 are directly involved in determining C_i, but the C_i are also dependent on V; on the other hand, V can be determined through 2 or 3, but these are dependent on the distribution and motion of charged molecules. For a given physiological process within a given time scale, however, some of these components may remain constant and therefore may not have to be explicitly considered.

Component 1 is the molecular flux, $\vec{\mathbf{J}}_i$, arising from diffusion and electric forces as described in the Nernst-Planck equation (Eq. 1) (Hille, 1992). Note that the subscript, i, denotes values pertaining to the ith molecular species:

$$\vec{J}_i = -D_i \nabla C_i - z_i \mu_i C_i \nabla V, \quad \mu_i = \frac{D_i F}{RT} \tag{1}$$

C_i is the concentration, D_i is the diffusion constant, z_i is the ionic valence, μ_i is the mobility, V is the electric potential, F is Faraday's constant, R is the gas constant, and T is the absolute temperature. The first term of Eq. 1 describes the diffusion flux, and the second term of Eq. 1 describes the flux due to the electric field. The latter will only be important for very fast physiological processes (e.g., action potentials) or very high spatial resolutions.

The time rate of change of concentration defined over an infinitesimally small volume is the sum of the net flux into the volume and the net reaction rate,

$$\frac{\partial C_i}{\partial t} = -\nabla \cdot \vec{\mathbf{J}}_i + S_i(C_1, C_2, \ldots C_N) \tag{2}$$

where the molecular flux, $\vec{\mathbf{J}}_i$, is defined by Eq. 1, and S_i defines the net chemical reaction rate for species i (component 4). For a chemical species produced in an aqueous compartment by a single chemical reaction, S_i is given by a simple rate equation, as exemplified by the common reversible reaction in Eqs. 3 and 4:

$$A + B \underset{k_{-1}}{\overset{k_1}{\rightleftharpoons}} C \tag{3}$$

$$S_C = k_1[A][B] - k_{-1}[C] \tag{4}$$

For a molecular species created or consumed in a number of reactions, S_i is simply the sum of the individual rate laws. The physical infrastructure deals separately with molecular fluxes through membranes (component 5, above), treating them as boundary conditions between two features that can also be functions of all concentrations and potentials. Thus the dependence of C_i on the concentration of all of the other molecular species is explicitly considered for both passage through membranes (e.g., ligand-gated channels) and production or consumption of species i in chemical reactions (e.g., enzyme-mediated transformations or buffer on/off rates).

$\vec{\mathbf{D}}$ and $\vec{\mathbf{I}}$ (components 2 and 3) are actually redundant alternatives for describing the electrical potential based on the instantaneous distribution of charge or the mobilities of charged molecules, respectively. The former is quite rigorous but requires small time steps to ensure convergence. The electric current density formulation permits an approach similar to the cable theory used in neuronal modeling, which assumes that the physiological processes of interest are slow compared to charge relaxation in the conductive aqueous compartments. Details of both of these alternative formulations for the electrical potential are provided in the Appendixes.

CHEMICAL DYNAMICS COMPUTATION

A key attribute of the Virtual Cell is the utilization of empirical three-dimensional data and images to directly build the simulation geometry. The anatomical features of the cell are identified and extracted as geometrical descriptions. These geometrical descriptions are sampled to create a simulation volume. This simulation volume represents a spatially heterogeneous collection of three-dimensional elements, in which each element pairs a subcellular anatom-

ical feature with its associated physiology. The spatial organization of cellular structure and function thus comprises a collection of feature models. These cellular features can be identified by three-dimensional segmentation of digital confocal or electron microscopy data. For cellular structures that are either too small or too convoluted to be extracted easily from actual data, feature geometry may be approximated by synthetic geometry. This synthetic geometry can consist of any combination of geometric primitives (e.g., sphere, cylinder), mathematically defined solid models (e.g., fractal solids), or arbitrary polygonal surfaces (e.g., CAD models).

The specification of the chemical dynamics is also very flexible. The simulation description specifies the molecular species to be simulated, the number of elements in each dimension, the size of the elements, and the simulation time step. The dynamics are described as time-dependent concentrations within elements and fluxes of molecular species across boundaries separating adjacent elements. These can be functions of diffusion, ion drift, potential, chemical reaction, or any other relationship involving the spatial distribution of molecular species. Membranes are represented by element boundaries separating dissimilar elements. The output of the simulation provides the time course for the concentrations of each molecular species within each element, the electric potential in each element, and the surface densities of the states of membrane-associated molecules. An object-oriented hierarchical scheme, summarized in Table 1, is used to organize the components needed to describe the physiological events under investigation.

Membrane reaction models and local reaction models are maintained as reaction descriptors set to define the reaction rates of molecular species as a function of the local environment. Each descriptor consists of a set of rate expressions that are functions of model variables and parameters (e.g., rate constants, channel conductances, etc). These descriptions are stored in a data base, and when needed, a specific model object library is automatically generated for input to a simulation. Thus new models may be specified with little exposure to the underlying numerical methods. In addition, this object-oriented approach lends itself well to the development of a data base of reaction and feature models that can be readily merged with a data base of cellular and subcellular images.

The numerical solution to the set of partial differential equations is achieved by the finite-volume method (Patankar, 1980). This method is based on the subdomain formulation of the method of weighted residuals, although the resulting discrete equations resemble those of the finite-difference method. The finite-volume method allows for very good control of boundary conditions and profile assumptions while preserving the conservative nature of many of the equations of interest (e.g., Fick's law and Gauss' law). Most importantly, finite-volume formalism accommodates the heterogeneous spatial organization of cellular compartments.

TABLE 1 Hierarchical organization of cellular components

Component	Description
Cell model	A collection of feature models organized in space to correspond to their organization in experimental or idealized images.
Feature model	A list of initial conditions, reaction models, membrane reaction models, and species parameters (ionic charges, diffusion coefficients) associated with a particular anatomical feature (e.g., cytosol feature model).
Reaction model	Mechanisms for individual biochemical transformations with their associated rate constants corresponding to reactions associated with molecules "in solution" (e.g., calcium buffering).
Membrane reaction model	Equations that represent reactions and fluxes associated with membrane molecules, including all relevant conductances and rate constants (e.g., G-protein cascades; calcium-induced calcium release through the ryanodine receptor)
Molecular species	A molecule or a distinct conformation of a molecule that is typically present "in solution" (e.g., cAMP, calcium ion). A state variable that represents a molecular species is defined in each element and holds the concentration of that species.
Membrane molecular species	A molecule or a distinct conformation of a molecule that is present only within a membrane (e.g., open conformation of a ryanodine receptor). A state variable that represents a membrane molecular species is defined only for elements that contain membranes and holds the surface density of that species.

The fundamental step in the numerical formulation involves integrating the equations in time over a single volume element, using appropriate interpolation profiles and boundary conditions. The solution of each integration relates a small neighborhood of sample values over space and time. The resulting equations are solved iteratively by the line-by-line method (Patankar, 1980). This is an implicit method that guarantees stability, given the physically appropriate constraints associated with physiological models. The ability of each iteration to converge to the solution of the nonlinear equations is made possible by an implicit underrelaxation scheme. The simulation geometry is composed of uniformly sampled orthogonal elements (cubes). Piecewise linear interpolation functions are used to interpret the values of molecular concentrations and electric potentials between element centers.

Within such uniformly sampled orthogonal elements, the time dependence of C_i is simply the sum of fluxes entering the volume element from its six adjacent neighbors plus the

production of molecular species i via reactions. In particular, as depicted in Fig. 1, the discretized form for the flux component of Eq. 2 between similar elements is simply

$$-\oint_S \vec{\mathbf{J}}_i \cdot d\vec{\mathbf{S}} = \text{Area}_{\text{boundary}} \cdot [J_x|_{x+} - J_x|_{x-} + J_y|_{y+} - J_y|_{y-} + J_z|_{z+} - J_z|_{z-}]_i \quad (5)$$

(For boundaries between dissimilar elements, membrane transport mechanisms are incorporated, as will be detailed below.) The x, y, and z components of the molecular flux J_x, J_y, and J_z are evaluated at the six element boundaries by assuming them to be constant across each boundary surface. The molecular fluxes depend on the element boundary conditions as summarized in Table 2. The simulation boundary conditions of either fixed concentration, or of fixed molecular flux, are easily applied. Similar discrete formulations for electric flux density and electric current density are detailed in Appendix II.

In general, the reaction rate for either elementary or multistep reactions is a nonlinear relation that may be linearized about a set of current conditions for sufficiently small time steps:

$$S_A \approx -f_{A\_linear}([A], [B], \dots) \cdot [A] + f_{A\_constant}([C], [D], \dots) \quad (6)$$

A particular simulation may not define one or more of the reagents as state variables. The reaction model must then either be disabled or simplified, depending on which reagents are missing. A simplified model uses a constant concentration for each missing reagent as defined for that biological feature type. This constant concentration can be specified in the reaction model description, or the default value for that feature type will be used.

TABLE 2 Discrete formulation for molecular flux

Boundary condition	Discrete approximation for molecular flux
Interface between similar elements	$J_x\|_{x+} = -D_i\nabla C\|_{x+} - z_i\mu_i C_i \nabla V\|_{x+} = D_i \dfrac{C_i(x) - C_i(x+\Delta x)}{\Delta x} + z_i\mu_i \cdot C_i\|_{x+} \cdot \dfrac{V(x) - V(x+\Delta x)}{\Delta x}$
Interface between dissimilar elements (membrane)	$J_x\|_{x+}$ = flux due to membrane transport $= f(C_1, C_2, \dots C_N, V)$
Simulation boundary (specified concentration)	Flux need not be evaluated
Simulation boundary (specified flux)	$J_x\|_{x+} = J_{\text{boundary}}$

As in the case of the solution reaction models, all-membrane reactions are treated as coupled differential equations describing their kinetics. However, the surface densities of the membrane molecular species can dictate the fluxes of solution molecular species through a "membrane," operationally defined within the Virtual Cell as a boundary between dissimilar elements. Membrane reaction models relate the transactions controlled by the membrane to the accessible states of receptors, pumps, channels, or carriers. This is illustrated for the open, closed, and inactive states of a prototypical three-state channel selective for solute S_1 in Fig. 2. The state transitions are defined in terms of reaction rate equations that can be functions of membrane potential and species concentrations on either side of the membrane. The equations are written such that the stoichiometry of the whole model is consistent and flux is conserved. These

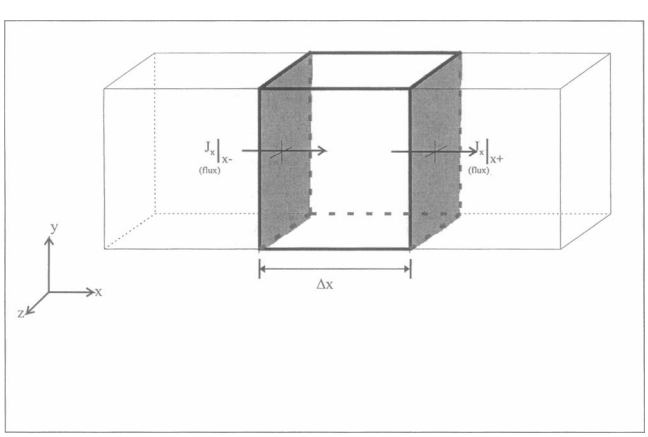

FIGURE 1 Finite volume formulation. Boundary conditions for individual elements in the chemical simulation framework guarantee mass conservation. The flux is calculated by the Nernst-Planck equation when the neighboring elements are of the same type. The flux is based on membrane reactions (channels, pumps. . .) when the neighboring elements are different. The y and z components of the flux are omitted for clarity.

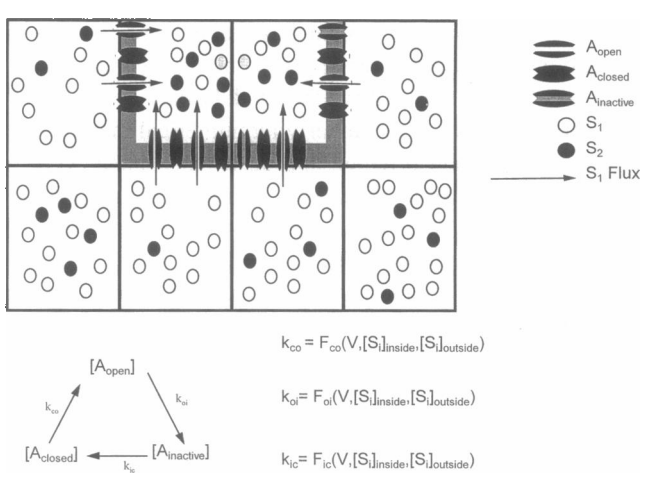

FIGURE 2 Transitions of membrane-bound molecules. This illustration of membrane reactions is based on a three-state model for a gated channel that controls the flux of solute S_1. The rate constants for opening, k_{co}, inactivation, k_{oi}, and activation, k_{ic}, can each be functions of membrane potential, V (voltage-gated channel), or the concentrations of ligands, S_i (chemically gated channel).

states are defined in terms of membrane surface densities and can be represented by state variables or by constants. There is only one value of the surface density of a membrane variable that is defined for each element, although an element may have up to six separate membrane surfaces. Reaction rates for each membrane reaction model are averaged over the membrane surfaces of an element. Missing reagents are handled in a manner similar to that of the bulk reactions defined above. An important additional requirement of the transmembrane reactions is that flux be conserved.

A primary application of the cell models is to investigate the course of events after a homeostatic system is perturbed by some stimulus. A cell model is constructed with a set of initial conditions corresponding to a best guess for the prestimulus values of the state variables, i.e., all concentrations, surface densities, and potentials. Some of these represent experimentally measured and estimated values, whereas others may not be known a priori. However, this guess may not represent a real steady state once all of the components of the model are permitted to interact. When an integrated cell model is built from an arbitrary collection of individual reaction models, care must be taken to achieve a self-consistent initial condition. Starting at a steady state allows consideration of the system's response to the stimulus without interference from the relaxation of initial conditions.

In general, there is not a unique steady state defined by the system and boundary conditions alone, but by fixing the values of the set of known variables to their prestimulus homeostatic values, it might be possible to allow the dynamic simulation to run until the desired steady state is reached. However, this could be wasteful of computer time. Moreover, the proposed cell model will not necessarily have a steady-state solution that is consistent with that fixed set of initial conditions. In this case either the initial conditions or the cell model must be modified.

A better and more direct approach involves the minimization of the initial dynamics (i.e., finding a steady-state equilibrium). The general method used to address this issue is nonlinear constrained optimization. The extent to which the system can be altered may be formalized by adding constraints or ranges for the undetermined or underdetermined initial values and system parameters. The measure of initial dynamics is a function of the magnitude of net reaction rates and fluxes for all species, where the steady state represents a system in which the time rate of change of each species is zero. The minimum solution arrives at parameter values and initial conditions simultaneously.

The problem becomes manageable if the system is first simplified by assuming that each species is homogeneous within the bounds of a feature. This reduces the problem to the constrained minimization of a system of nonlinear algebraic equations. An initial implementation uses a conjugate gradient method for the minimization of the system dynamics and a penalty function associated with the violation of constraints (Bryson and Ho, 1975). Although necessary for finding the proper initial conditions before stimulation, the ability to test how a subset of physiological parameters relaxes to a steady state is also of great value in evaluating hypotheses on the interrelations of complex cellular processes.

EXAMPLE MODEL: CALCIUM WAVE IN A NEURONAL CELL

The origin, regulation, and role of calcium as a second messenger in intracellular signal transduction is a subject of intense investigation (Berridge, 1993). The complexity of the interacting and varied mechanisms that have been discovered at the biochemical and electrophysiological levels makes models for calcium dynamics a good initial test for the usefulness of the Virtual Cell approach. We have constructed a limited cell model based on inositol-1,4,5-trisphosphate (IP_3)-mediated calcium waves in differentiated N1E-115 neuroblastoma cells. In these cells, the peptide hormone bradykinin triggers calcium waves that are known to involve the IP_3 receptor on the endoplasmic reticulum (ER) membrane, without involvement of the ryanodine receptor or calcium influx through plasma membrane channels (Monck et al., 1990; Wang and Thompson, 1995). Thus only calcium release through the IP_3 receptor channel need be considered in our model.

The state variables and initial conditions associated with the features of the cell model are given in Table 3. An effective diffusion constant for calcium of 40 $\mu m^2/s$ is chosen to implicitly account for calcium buffering in the cytosol (Jafri and Keizer, 1995). To initiate a calcium response, the bradykinin is stepped to the saturating level of 500 nM at $t = 0$ (although bradykinin is assigned a diffusion coefficient, its concentration is uniform, so its flux is 0 throughout the extracellular space). A two-state bradykinin receptor model in the plasma membrane then responds with an initial burst of 5000 molecules $IP_3/\mu m^2 \cdot s$ that exponentially relaxes to a steady-state production of 100 molecules of $IP_3/\mu m^2 \cdot s$ with a time constant of 50 ms. The ER feature model contains a five-state membrane reaction model for the type 1 IP_3 receptor, for which the most detailed kinetic parameters are available in the literature (Bezprozvanny et al., 1991; Bezprozvanny, 1994; Bezprozvanny and Ehrlich, 1994). This membrane reaction model is fully detailed in Fig. 3. The sarcoplasmic/endoplasmic reticulum calcium ATPase pump (SERCA pump) is a second membrane reaction model that is part of the ER feature model. This is set to pump calcium back into the ER with a calcium dependence given by Eq. 7 (Lytton et al., 1992; Sneyd et al., 1995):

$$J = V_{max}[\text{SERCA}] \frac{[Ca^{2+}]_{cyt}^2}{K^2 + [Ca^{2+}]_{cyt}^2} \tag{7}$$

where V_{max} is taken as 2.52×10^{-2} ($\mu M \cdot \mu m^3$)/pump $\cdot$ s), [SERCA] is given in units of pumps/μm^2, and K, the

TABLE 3 Components of the neuroblastoma cell calcium wave model

Feature	Species	Initial condition	Diffusion coefficient
ER	$[Ca^{2+}]$	2500 μM	40 $\mu m^2/s$
	R, IP_3 Receptor (unbound)	9.43026 chan/μm^2	—
	RI, IP_3 Receptor (with IP_3)	0.14145 chan/μm^2	—
	RIC, IP_3 Receptor (with IP_3 & 1 Ca)	0.02768 chan/μm^2	—
	RICC, IP_3 Receptor (with IP_3 & 2 Ca)	0.39890 chan/μm^2	—
	RIC_Open, IP_3 Receptor (with IP_3 & 1 Ca, Open)	0.00171 chan/μm^2	—
	SERCA pump	5×10^3 pump/μm^2	—
Cytosol	$[Ca^{2+}]$	0.05 μM	40 $\mu m^2/s$
	$[IP_3]$	0.01 μM	250 $\mu m^2/s$
	Bradykinin receptor (unbound)	200 receptor/μm^2	—
	Bradykinin receptor (bound)	0 receptor/μm^2	—
Extracellular	[Bradykinin] (stimulus)	0 μM, $t = 0$; 0.5 μM, $t > 0$	100 $\mu m^2/s$

half-saturation concentration for calcium binding to SERCA, is taken as 270 nM.

The model was completed by using an experimental confocal micrograph of a differentiated neuroblastoma cell as the basis for the geometric distribution of cytosolic elements and ER elements. The ER in the cell was visualized by microinjecting a soybean oil solution of the fluorescent dye di-18:2-1-(3-sulfanatopropyl)-4-[β-[2-dilinoleylamino)-6-naphthyl]vinyl]pyridinium betaine) (ANEPPS) (synthesized by Joseph Wuskell according to methods developed in our laboratory (Hassner et al., 1984; Tsau et al., 1996) and available from Molecular Probes, Eugene, OR) according to the procedure developed by Terasaki et al. (Terasaki and Jaffe, 1991). A confocal image of such a cell is displayed in Fig. 4, along with the derived distribution of elements associated with intracellular features. The distribution of ER elements was set in proportion to the density of ER visualized in the confocal image, with a high density in the cell soma and a lower density in the neurite and

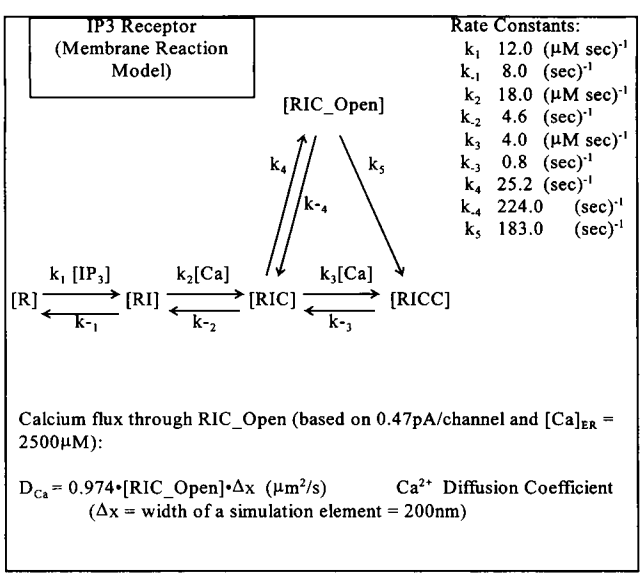

FIGURE 3 IP3 receptor membrane model based on the model of Bezprozvanny et al. (Bezprozvanny et al., 1991; Bezprozvanny and Ehrlich, 1994).

growth cone; the ER was excluded from the region defined by the cell nucleus, but a nucleus feature model was not separately defined. Although the elements were defined as three-dimensional cubes 200 nm on a side, only one plane of elements was employed for the computation, with dimensions of 54 μm $\times$ 20 μm $\times$ 0.2 μm; thus the cell model was effectively two-dimensional.

A 2-s simulation was generated with a time step of 100 μs. The first 1.6 s of the simulation was sampled at 200-ms intervals (Fig. 5). The ER elements correspond to the white pixels in the $t = 0$ calcium image, as the pseudocolor scheme maps the luminal ER $[Ca^{2+}]$ of 2.5 mM to white. A most useful feature of the Virtual Cell is the ability to visualize the dynamics of intracellular components, such as $[IP_3]$ and IP_3R in Fig. 5, that are not accessible experimentally. The IP_3 concentration is seen to build up rapidly in the neurite, resulting in a nucleation point for a calcium wave at $t = 200-400$ ms. Ca^{2+} fills the entire neurite within 100 ms and rapidly declines, except for a wavefront that gradually migrates into the soma. The pattern and speed of these calcium dynamics are similar to those found experimentally (Wang and Thompson, 1995; Fink et al., unpublished results). A key conclusion from this simulation is that the calcium wave can originate in the neurite, even when the density of plasma membrane hormone receptors is uniform and when the density of ER is actually higher in the soma. This is the pattern consistently observed experimentally (Fink et al., unpublished results; cf. http://www2.uchc.edu/htbit). As revealed in Fig. 5, it can be explained by the more rapid buildup of $[IP_3]$ in the neurite, where the surface-to-volume ratio, and therefore the rate of production of IP_3, is higher than in the soma. This factor overrides the higher density of IP_3 receptor in the soma dictated by the higher density of ER. It is also clear that the calcium signal decays rapidly, despite the continuous buildup of IP_3 in our rudimentary model. This can be understood by the combined action of SERCA pumps and the negative feedback on channel open probability associated with the RICC state in the five-state model of Fig. 3. Indeed, the drop in $[Ca^{2+}]$ allows the IP_3R to partially recover and permit a secondary, highly damped calcium rise in the neurite to appear at $t =$ 800 ms. Although a more realistic reaction model for IP_3

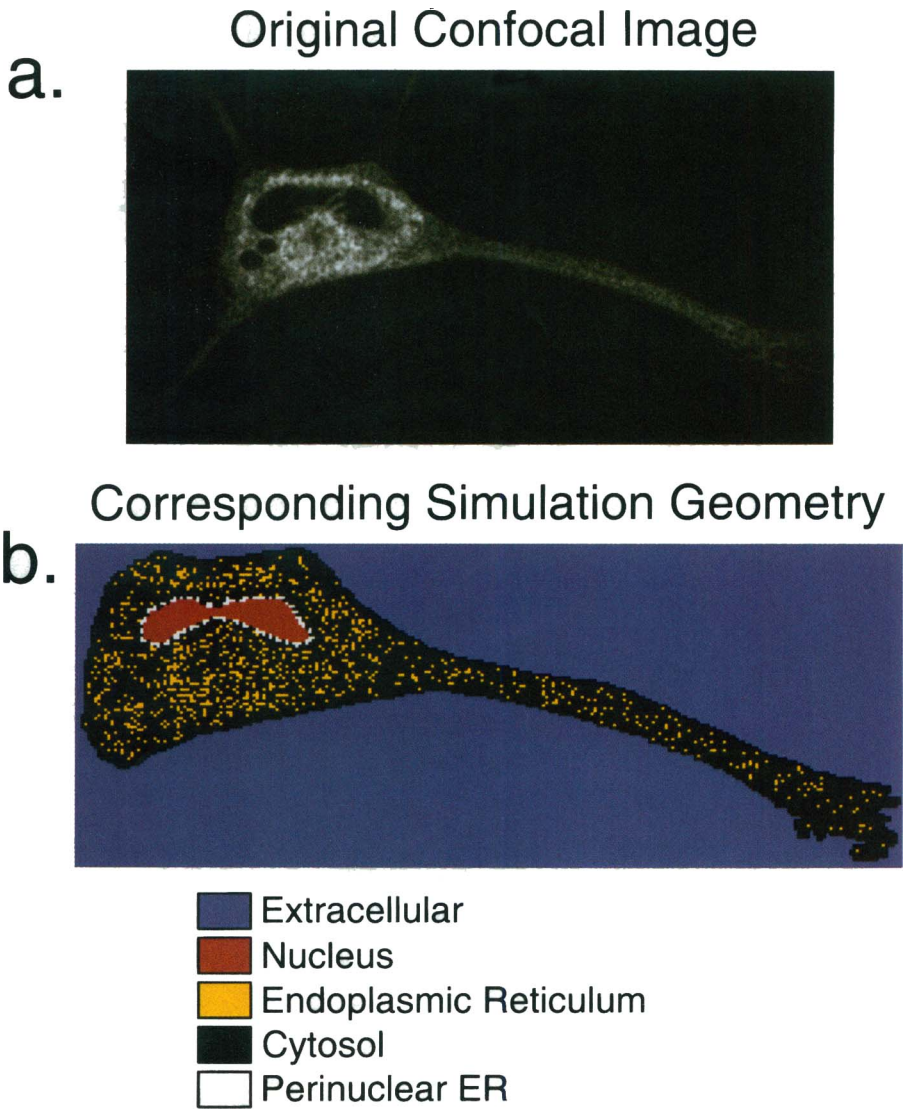

FIGURE 4 Derivation of cell model for neuronal calcium signaling from a confocal micrograph of an ER labeled cell. (*a*) A differentiated N1E-115 neuroblastoma cell was microinjected with di-18:2-ANEPPS dissolved in soybean oil, and the fluorescent dye was allowed to diffuse from the oil droplets into the ER for 1 h. The displayed image was chosen to represent an optical slice fully within both the neurite and soma. The ER has its highest density in the soma, with a more diffuse distribution in the neurite and growth cone. The kidney-shaped dark region in the soma is the nucleus, and the two small dark circles are the injected oil droplets (now free of dye). (*b*) The image in *a* was segmented and classified by simple thresholding techniques to define the indicated cellular and extracellular regions. The segmented image was then sampled at a lower pixel density to limit the mesh resolution for the simulation geometry. To eliminate the obvious experimental artifact, a few ER elements were added manually to the region obscured by the oil droplets. The small neurites projecting from the top and left of the soma were omitted to reduce the computational size of the simulation.

production and decay would have to be incorporated to try to fully simulate experimental behavior and verify such subtle effects as damped oscillations, it is revealing that only the cell geometry, the properties of the IP_3 receptor, and the presence of the SERCA pump can suffice to produce calcium waves with the essential spatial and temporal features observed experimentally. Furthermore, the example model is uses too coarse a mesh to resolve microdomains around channels; however, higher spatial resolution, perhaps while using only a small fragment of a cell, could help elucidate the dynamics of calcium close to the ER membrane.

DISCUSSION

Most current approaches to the modeling of cellular physiology are based on highly restricted sets of biochemical reactions and idealized geometries, and include many other simplifying assumptions. Cells are represented as simple geometrical shapes consisting of spatially homogeneous behavior. Significant insights can be attained with such approaches as exemplified by detailed simulations of intracellular calcium dynamics (Atri et al., 1993; Jafri, 1995; Jafri and Keizer, 1995; Sneyd et al., 1995; Dupont and Swillens, 1996; Keizer and Levine, 1996; Smith, 1996; Smith et al., 1996; Wu et al., 1996). However, such formulations preclude the expression of an observed physiological phenomenon as it maps to the actual geometry of an intact cell. Thus features of the physiology that depend on the spatial organization of molecules within and between cellular organelles cannot be accommodated by current methods.

There have also been numerous simulations in neurophysiology involving formulations based on cable theory (Hodgkin and Huxley, 1952; Jack et al., 1975a; Hines, 1989; Smith, 1992). These decompose a single neuronal cell into branching cylindrical computational elements representing axons and dendrites. Although these simulations reproduce neuronal transmission with good fidelity, the inherent geometric simplicity of the formulation restricts their application to the class of problems in which the cell interior is considered a homogeneous conductive medium.

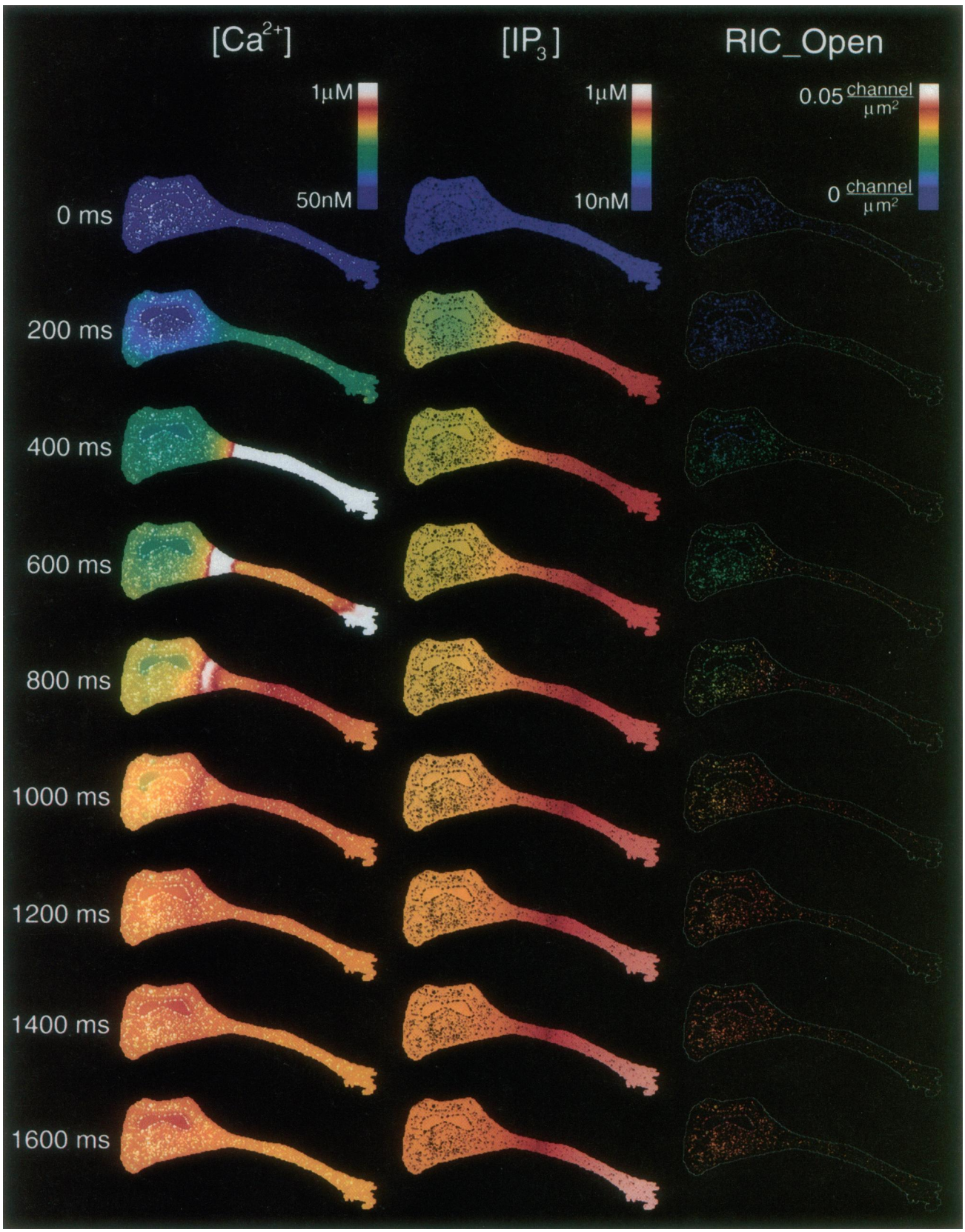

FIGURE 5 Dynamic simulation of intracellular signaling in a neuronal cell. The cell model specified by Figs. 3 and 4 and Table 3 was used as the input for a dynamic simulation with time steps of 100 μs. The results are shown at 200-ms intervals for three of the state variables: $[Ca^{2+}]$ (*left*), $[IP_3]$ (*center*), and the density of open IP_3 receptor channels (*right*). The latter are only associated with the ER and are displayed with a white outline of the cell to aid visualization. The $[Ca^{2+}]$ and $[IP_3]$ pseudocolor scales are logarithmic, and the RIC_Open scale is linear.

It is difficult to extend this approach to the simulation of intracellular ion dynamics, for example. Furthermore, specialized structures such as boutons or spines are necessarily beyond the scope of methods based on linear cable theory.

We have developed a comprehensive, extensible, and flexible framework ("Virtual Cell") for organizing, modeling, simulating, and visualizing cell structure and physiology. The spatial organization of cellular components is captured by incorporating geometries from volume data sets. These data may be derived from experimental micrographs or may be synthesized. Each geometrical feature is identified as a specific cellular compartment and associated with a mathematical model that represents its function in a cell. A chemical dynamics simulation is created by sampling the geometry into a three-dimensional mesh of simulation elements. The approach uses a finite-volume formalism that assigns appropriate properties (starting concentrations of chemical species, diffusion constants, ionic charges, reaction rates, etc.) to elements identified with the different compartments involved in the process. Boundaries between compartments are given the properties of the corresponding membranes, including channels, pumps, receptors, etc. The partial differential equations of electrodiffusion, plus source terms corresponding to reactions, are solved for each chemical species and electric potential in each volume element. The formulation is sufficiently general that any mechanism for a dynamic physiological process can be modeled over the domain represented by a three-dimensional image. Simulation elements, concentrations, electric potential, receptor and channel states, and original 3D images can be rendered into the same 3D scene, mapped to the same coordinate system for direct comparison, and are viewed as a time-dependent series of images displaying the intracellular chemical dynamics underlying the physiological response. The same physiological models can be verified in multiple experiments (different geometry and different stimuli). As related models are examined under various conditions and with different cell types, general themes will emerge and can be evaluated in a systematic way. Thus the Virtual Cell creates a framework for testing mechanistic hypotheses and encapsulating knowledge about the interactions and dynamics of intracellular components.

The finite-volume formalism (Patankar, 1980) is a special case of the method of finite difference (Smith, 1985; Mascagni, 1989) that has been successful in simulations of large complex systems such as heat transfer, fluid mechanics, astrophysics, geology, or global climate patterns (Sellers et al., 1997). These problems are similar to the Virtual Cell in that they require the solution of a series of ordinary and partial differential equations with structures equivalent to those describing electrodiffusion with source terms. The Virtual Cell may be unique, however, in the sheer number and variety of such equations that are potentially required to describe a cell physiological system. Furthermore, the treatment of membranes within the finite-volume formalism was a particular challenge. To capture the relative scale of a fully defined membrane feature, the mesh size would have to be set at a prohibitively fine resolution. A novel aspect of our formulation for the Virtual Cell is the treatment of membranes as discontinuities at boundaries between elements associated with different features. This permits us to deal explicitly with the properties of membranes without having to define them as separate features.

The current implementation of the Virtual Cell uses structured input files, each representing separate reaction models and feature models. The input includes initial conditions for each of the molecular species, rate constants for each of the reaction steps, and, for the case of membrane reaction models, permeabilities or conductances in addition to the relevant reaction rates. The model objects are generated and compiled automatically from these input files. A cell model is then created based on the spatial organization of the features derived from appropriately segmented experimental images. During the course of a computation, values of the state variables are periodically stored to files that uniquely represent the simulated physiology at a discrete point in time. Any state variable can then be visualized over space and time by reading these files, with their associated geometrical models, into a 3D viewer. Fig. 5 is an example of the display of the time dependence of three state variables as a collage, but the 3D viewer can also be used to generate movies. In addition, the state variables can be used in postprocessing of the data to determine derived states. Such derived states can be reaction rates, fluxes, or other functions of state variables that are explicitly or implicitly represented in the constituent models.

It is important to realistically assess the magnitude of the computational power required for the Virtual Cell. The computation in our example simulation was of a relatively modest 2D cell model containing a limited number of reaction models and molecular species. The computations behind Fig. 5 comprised 27,000 elements, three nonlinear partial differential equations, and seven nonlinear ordinary differential equations. This cell model required only the solution of the diffusion and source equations; it did not include the electric potential formulation. The 2-s simulation required 2 days of computation on a Silicon Graphics workstation using a R8000 MIPS cpu rated at 300 Mflops. Although this system is only 1 year old, faster desktop workstations are already available that will improve the speed by at least a factor of 3, and supercomputers can be expected to speed up the calculation still further. Furthermore, the numerical methods used in the first implementation are conservative, and have not been adapted to run on multiprocessor systems. These can be replaced with more efficient methods that can be made parallel in anticipation of improvements in processing speeds of several orders of magnitude. Thus much more complex cell models may be realistically accommodated in the next generation of implementation.

The modular object-oriented structure of the framework will permit the next implementation to include a graphical user interface and will support the compilation of a data

TABLE 4 Discrete formulation for electric flux density

Boundary condition	Discrete approximation for electric flux density, **D**
Interface between similar elements	$\mathbf{D}_x\|_{x+} = -\nabla V\|_{x+}\varepsilon = \frac{V(x) - V(x+\Delta x)}{\Delta x}\varepsilon$
Interface between dissimilar elements (capacitive membrane)	$\mathbf{D}_x\|_{x+} = -\nabla V\|_{x+}\varepsilon = \frac{V(x) - V(x+\Delta x)}{\text{membrane } \Delta x}\varepsilon_{\text{membrane}}$
Simulation boundary (specified voltage)	**D** need not be evaluated
Simulation boundary (specified field)	$\mathbf{D}_x\|_{x+} = \varepsilon_{x+} Ex = \varepsilon Ex$

base of reaction models and feature models. Together with a library of images, combinations of feature models can generate cell models for different cell types and physiological problems. A data base of specific and customizable reaction and membrane mechanisms can be made available for building cellular models through a central repository. Such a repository of models could be maintained at a World Wide Web site. A naming standard for both models and molecular species must be created to allow models to be interoperable. Run-time binding of a model object library to the simulation allows a single version of the simulation framework to service any simulation with recompilation of only the newly specified models.

We will also need to focus on several issues to increase the range of problems to which the Virtual Cell may be applied. The current treatment of membrane channel and pump surface densities assumes a single value for each element, representing the average over all of that element's membrane boundaries; this will have to be modified to account for heterogeneously distributed two-dimensional membrane patches. The approach may be easily extended to phenomena involving intercellular interactions with very little change in the basic formulation. A greater challenge is posed by processes involving changes in cell shape or dynamic changes in the location or number of intracellular organelles. Such processes will not necessarily be fully covered by the physical laws of electrodiffusion. Additional physical formulations will be required and coupled with algorithms that incorporate deformable volume elements and/or methods by which elements may be variably associated with feature models. Thus the Virtual Cell should be able to accommodate cell models describing any cellular process. But the availability of such models will ultimately depend on the continued generation of experimental data describing the elementary components of cellular biochemistry, biophysics, and physiology.

APPENDIX I

Electric potential equations

An approach based on electrostatics (Gauss's Law)

For charged molecules, Eqs. 1 and 2 show that the time dependence of C_i is also dependent on V. However, V is itself dependent on the distribution of charged molecules and structures. The electric potential can be defined according to the laws of electrostatics, using Gauss's law (A1), which states that the net charge, Q, within a closed surface is equal to the net electric flux density, $\vec{\mathbf{D}}$, leaving that surface (Hayt, 1981):

$$Q = \oint \vec{\mathbf{D}} \cdot d\vec{S} \tag{A1}$$

$\vec{\mathbf{D}}$ is related to the permittivity (or dielectric constant) (ϵ), the electric field ($\vec{E}$), and the electric potential (V) according to

$$\vec{\mathbf{D}} = \varepsilon E = -\varepsilon \nabla V \tag{A2}$$

The total charge within a volume can be defined as the concentration of molecular species, C_i, the ionic valence, z_i, and Faraday's constant, F, integrated over that volume:

$$Q = \oint_v \left[\sum_i z_i F C_i\right] dv \tag{A3}$$

Combining these three equations gives a form of Gauss's Law (Eq. A4) that can be evaluated for an incremental volume and relates electric potential to ionic concentrations:

$$\oint_v \left[\sum_i z_i F C_i\right] dv = \oint_S (-\varepsilon \nabla V) \cdot d\vec{S} \tag{A4}$$

An approach based on electric currents

The electric potential can also be defined as a function of electric currents through a conductive medium and across capacitive boundaries (Hodgkin and Huxley, 1952; Jack et al., 1975b). Conservation of charge states that in a conductor, the net current density, $\vec{\mathbf{I}}$, leaving any closed surface, $d\vec{S}$, is equal to 0:

$$-\frac{dQ}{dt} = \oint_S \vec{\mathbf{I}} \cdot d\vec{S} = 0 \tag{A5}$$

This formulation assumes that the interior of all connected regions within a component (cytosol, organelle lumen, extracellular milieu, etc.) can be modeled as conductors or, equivalently, that the relaxation of a free charge from the interior to the surface (membrane) is much faster than the cellular dynamics of interest. $\vec{\mathbf{I}}$ can be related to the electric potential V by

TABLE 5 Discrete formulation for electric current density

Boundary condition	Discrete approximation for electric current density, J
Interface between similar elements	$\mathbf{I}_x\|_{x+} = -\lambda\nabla V\|_{x+} - F\sum_i z_i D_i \nabla C_i$ $= -\frac{\lambda(x)+\lambda(x+\Delta x)}{2}\cdot\frac{V(x)-V(x+\Delta x)}{\Delta x} + F\sum_i z_i f_i(\,)$
Interface between dissimilar elements (capacitance membrane)	$\mathbf{I}_x\|_{x+} = C_m\frac{\partial(V_m)}{\partial t} + F\sum_i z_i F_i 0$ $= C_m(V_x^{new} - V_{x+\Delta x}^{new}) - (V_x^{old} - V_{x\,old} - V_{x+\Delta x}^{old}\Delta t + F\sum_i z_i f_i(\,)$
Simulation boundary (specified voltage)	$\mathbf{I}_x\|_{x+}$ does not need to be evaluated
Simulation boundary (specified field)	$\mathbf{I}_x\|_{x+} = +\lambda\vec{E}\|_{x+} - F\sum_i z_i D_i\nabla C_i = +\frac{\lambda(x)+\lambda(x+\Delta x)}{2}$ $\cdot E_{boundary} - F\sum_i z_i D_i\frac{C_i(x)-C_i(x+\Delta x)}{\Delta x}$

expansion of Eq. 1:

$$\vec{\mathbf{I}} = F\sum_i z_i\vec{\mathbf{J}}_i = -\lambda\nabla V - F\sum_i z_i D_i\nabla C_i \qquad \text{where } \lambda = F\sum_i z_i^2\mu_i C_i \tag{A6}$$

The first term represents Ohm's law, and the second is the current density due to the concentration gradients. For a conductor (i.e., extracellular milieu, cytosol, or organelle lumen), the component of current density normal to a membrane, $\mathbf{I}_n$, is related to the membrane-specific capacitance, C_m, the potential drop across the membrane, ΔV_m, and the net charge flux density passing through the membrane, $\mathbf{I}_m$ (via pumps, channels, etc.) according to

$$\mathbf{I}_n = -C_m\frac{\partial(\Delta V_m)}{\partial t} + \mathbf{I}_m \tag{A7}$$

Equations A5 and A6, and the membrane boundary condition (Eq. A7) give a form of conservation of current that can be applied to both membranes and interior spaces without the geometrical constraints of cable theory.

APPENDIX II

Discretization of electrical potential formulations

Electric flux density

Within an element, the left side of Eq. A4 becomes the sum of the average charges due to each molecular species. Assuming a linear profile of concentration between adjacent elements, the average concentration $\bar{C}_i$ over an element is computed as a linear combination of the sample concentration of the current element and its nearest neighbors:

$$\oint_v\left[\sum_i z_i F C_i\right]dv = \text{Volume}\cdot\sum_i z_i F\bar{C}_i \tag{A8}$$

$$\oint_S\vec{\mathbf{D}}\cdot d\vec{S} = \text{Area} \cdot h[\boldsymbol{D}_x|_{x+} - \boldsymbol{D}_x|_{x-} + \boldsymbol{D}_y|_{y+} - \boldsymbol{D}_y|_{y-} + \boldsymbol{D}_z|_{z+} - \boldsymbol{D}_z|_{z-}] \tag{A9}$$

Area and Volume refer to the size of a single element. The x, y, and z components of the electric flux density D_x, D_y, and D_z are evaluated at the six element boundaries by assuming them to be constant across each boundary surface. The electric potential of neighboring elements are then related by one of the forms of Table 4. The simulation boundary conditions of either fixed potential or fixed electric field (or electric flux density) are easily applied.

Electric current density

This formulation requires a representation for current density within the interior of a conductor as well as across membranes. Referring to Eq. A5, the sum of the electric current densities entering an element is due to each molecular species (Eq. A10). Assuming a linear profile of conductance between adjacent elements, the average conductance λ over an element is computed as a linear combination of the sample concentrations of the current element and its nearest neighbors.

$$\oint_S\vec{\mathbf{I}}\cdot d\vec{S} = \text{Area} \cdot [\mathbf{I}_x|_{x+} - \mathbf{I}_x|_{x-} + \mathbf{I}_y|_{y+} - \mathbf{I}_y|_{y-} + \mathbf{I}_z|_{z+} - \mathbf{I}_z|_{z-}] = 0 \tag{A10}$$

Area refers to the side of a single cubic element. The x, y, and z components of the electric flux density $\mathbf{I}_x$, $\mathbf{I}_y$, and $\mathbf{I}_z$ are evaluated at the six element boundaries by assuming them to be constant across each boundary surface. The electric potential of neighboring elements are then related by the appropriate entry in Table 5. The simulation boundary conditions of either fixed potential, or of fixed electric field (or electric flux density) are easily applied.

The authors are pleased to acknowledge valuable comments on the manuscript from James Watras, Mark Terasaki, Ann Cowan, Barbara Ehrlich, and Laurinda Jaffe.

Supported by grants from the U.S. Public Health Service (GM35063) and the State of Connecticut (Critical Technologies Program).

REFERENCES

Atri, A., J. Amundson, D. Clapham, and J. Sneyd. 1993. A single-pool model for calcium oscillations and waves in the *Xenopus laevis* oocyte. *Biophys. J.* 65:1727–1739.

Berridge, M. J. 1993. Inositol trisphosphate and calcium signalling. *Nature.* 361:315–325.

Bezprozvanny, I. 1994. Theoretical analysis of calcium wave propagation based on inositol(1,4,5)trisphosphate ($InsP_3$) receptor functional properties. *Cell Calcium.* 16:151–166.

Bezprozvanny, I., and B. E. Ehrlich. 1994. Inositol(1,4,5,)-trisphosphate ($InsP_3$)-gated Ca channels from cerebellum: conduction properties for divalent cations and regulation by intraluminal calcium. *J. Gen. Physiol.* 104:821–856.

Bezprozvanny, I., J. Watras, and B. E. Ehrlich. 1991. Bell-shaped calcium-response curves of $Ins(1,4,5)P_3$- and calcium-gated channels from endoplasmic reticulum of cerebellum. *Nature.* 351:751–754.

Bryson, J. A. H., and Y.-C. Ho. 1975. Applied Optimal Control. Hemisphere Publishing, New York. 39–41.

Dupont, G., and S. Swillens. 1996. Quantal release, incremental detection, and long-period Ca^{2+} oscillations in a model based on regulatory Ca^{2+}-binding sites along the permeation pathway. *Biophys. J.* 71:1714–1722.

Frost, A. A., and R. G. Pearson. 1961. Kinetics and Mechanism. John Wiley and Sons, New York.

Hassner, A., D. Birnbaum, and L. M. Loew. 1984. Charge shift probes of memrane potential. *Synthesis J. Org. Chem.* 49:2546–2551.

Hayt, W. H., Jr. 1981. Engineering Electromagnetics. McGraw-Hill, New York. 57–176.

Hille, B. 1992. Ionic Channels of Excitable Membranes. Sinauer Associates, Sunderland, MA.

Hines, M. 1989. A program for simulation of nerve equations with branching connections. *Int. J. Biomed. Comput.* 24:55–68.

Hodgkin, A. L., and A. F. Huxley. 1952. A quantitative description of membrane current and its application to conduction and excitation in nerve. *J. Physiol. (Lond.).* 117:500–544.

Jack, J. J. B., D. Noble, and R. W. Tsien. 1975. Electric Current Flow in Excitable Cells. Clarendon Press, Oxford.

Jafri, M. S. 1995. A theoretical study of cytosolic calcium waves in *Xenopus* oocytes. *J. Theor. Biol.* 172:209–216.

Jafri, M. S., and J. Keizer. 1995. On the roles of Ca^{2+} diffusion, Ca^{2+} buffers, and the endoplasmic reticulum in IP_3-induced Ca^{2+} waves. *Biophys. J.* 69:2139–2153.

Keizer, J., and L. Levine. 1996. Ryanodine receptor adaptation and Ca^{2+}-induced Ca^{2+} release-dependent Ca^{2+} oscillations. *Biophys. J.* 71: 3477–3487.

Lytton, J., M. Westlin, S. E. Burk, G. E. Shull, and D. H. MacLennan. 1992. Functional comparisons between isoforms of the sarcoplasmic or endoplasmic reticulum family of calcium pumps. *J. Biol. Chem.* 267: 14483–14489.

Mascagni, M. V. 1989. Numerical methods for neuronal modeling. *In* Methods in Neuronal Modeling: From Synapses to Networks. C. Koch and I. Segev, editors. MIT Press, Cambridge, MA. 439–484.

Monck, J. R., R. E. Williamson, I. Rogulja, S. J. Fluharty, and J. R. Williamson. 1990. Angiotensin II effects on the cytosolic free Ca^{2+} concentration in N1E-115 neuroblastoma cells: kinetic properties of the Ca^{2+} transient measured in single fura-2 loaded cells. *J. Neurochem.* 54:278–287.

Patankar, S. V. 1980. Numerical Heat Transfer and Fluid Flow. Taylor and Francis, Washington, DC.

Sellers, P. J., R. E. Dickinson, D. A. Randall, A. K. Betts, F. G. Hall, J. A. Berry, G. J. Collatz, A. S. Denning, H. A. Mooney, C. A. Nobre, N. Sato, C. B. Field, and A. Henderson-Sellers. 1997. Modeling the exchange of energy, water, and carbon between continents and the atmosphere. *Science.* 275:502–509.

Smith, G. D. 1985. Numerical Solution of Partial Differential Equations: Finite Difference Methods. Clarendon Press, Oxford.

Smith, G. D. 1996. Analytical steady-state solution to the rapid buffering approximation near an open Ca^{2+} channel. *Biophys. J.* 71:3064–3072.

Smith, G. D., J. Wagner, and J. Keizer. 1996. Validity of the rapid buffering approximation near a point source of calcium ions. *Biophys. J.* 70:2527–2539.

Smith, R. G. 1992. NeuronC: a computational language for investigating functional architecture of neural circuits. *J. Neurosci. Methods.* 43: 83–108.

Sneyd, J., J. Keizer, and M. J. Sanderson. 1995. Mechanisms of calcium oscillations and waves: a quantitative analysis. *FASEB J.* 9:1463–1472.

Terasaki, M., and L. A. Jaffe. 1991. Organization of the sea urchin egg endoplasmic reticulum and its reorganization at fertilization. *J. Cell Biol.* 114:929–940.

Tsau, Y., P. Wenner, M. J. O'Donovan, L. B. Cohen, L. M. Loew, and J. P. Wuskell. 1996. Dye screening and signal-to-noise ratio for retrogradely transported voltage-sensitive dyes. *J. Neurosci. Methods.* 170:121–129.

Wang, S. S.-H., and S. H. Thompson. 1995. Local positive feedback by calcium in the propagation of intracellular calcium waves. *Biophys. J.* 69:1683–1697.

Wu, Y.-C., T. Tucker, and R. Fettiplace. 1996. A theoretical study of microdomains in turtle hair cells. *Biophys. J.* 71:2256–2275.